Acta Biomaterialia 89 (2019) 126–138

Contents lists available at ScienceDirect

Acta Biomaterialia

journal homepage: www.elsevier.com/locate/actabiomat

Full length article

Tissue-specific decellularized endometrial substratum mimicking different physiological conditions influences *in vitro* embryo development in a rabbit model

Hannes Campo [a], Ximo García-Domínguez [b], Sara López-Martínez [a], Amparo Faus [a], José Salvador Vicente Antón [b], Francisco Marco-Jiménez [b,1], Irene Cervelló [a,*,1]

[a] Fundación Instituto Valenciano de Infertilidad (FIVI), Instituto Universitario IVI/INCLIVA, Valencia, Spain
[b] Instituto de Ciencia y Tecnología Animal, Universitat Politècnica de València a, C/Camino de Vera s/n, 46022 Valencia, Spain

ARTICLE INFO

Article history:
Received 9 November 2018
Received in revised form 27 February 2019
Accepted 4 March 2019
Available online 5 March 2019

Keywords:
Tissue engineering
Decellularization
Endometrium
Embryo culture
ECM hydrogel

ABSTRACT

In the last decades, the decellularization (DC) of organs has become an established technique in the field of regenerative medicine to yield complex and vascularized bioscaffolds. Furthermore, it has been demonstrated *in vitro* that these decellularized scaffolds retain their native tissue-specificity. This is also the case when this tissue-specific extracellular matrix (ECM) is solubilized and used as hydrogels or coatings to create a biomimetic environment. In this study we investigated if this specificity not only remains when applied to distinct tissues but even more, that these differences can be distinguished within the same tissue at different stages of proliferation. To address this question, a sensitive *in vitro* animal model was used: rabbit embryos at the third day of development were cultured on coatings made from acellular endometrium that was non-proliferating (non-synchronous, NS) and proliferating (synchronous with the embryo, S) and their development was compared.

For this, we obtained whole NS and S rabbit uteri and subjected them to an adapted decellularization protocol. The acellular endometrium was carefully separated by microdissection and converted into a pre-gel solution to be used as hydrogels and coatings for *in vitro* assays. First, the characteristics of these NS and S hydrogels were investigated by proteomic analysis, electron microscopy and gelling kinetics. When used as substrata for day 3 embryos culture, it became apparent that only the acellular ECM from synchronous endometrial coating achieved similar results to the gold standard culture protocols and conditions, possibly because of the slow release of growth factors present in the synchronous/proliferating endometrium.

Statement of Significance

It has been shown by *in vitro* culture of stem cells, progenitor cells and primary culture cells that decellularized tissues retain their specific functions and biochemical and structural compositions. The present work demonstrates that using a mild SDS and perfusion based decellularization (DC) protocol not only effectively decellularize whole rabbit uteri, adding to the growing field of reproductive tissue engineering, but more importantly that the differences in the proliferating endometrium are translated after DC. This implies that DC not only retains the interspecificity of tissues but also the intraspecificity of a developing hormonally stimulated tissue. For the first time, we demonstrate that the coating from decellularized synchronous endometrium acts as a biological support for *in vitro* embryo development, achieving comparable results with the current gold standard that only uses serum-containing media.

1. Introduction

Current cell culture techniques are the result of gradual improvements over the years, recently one novel approach is focused on culture systems using tissue-specific extracellular

* Corresponding author.
E-mail address: Irene.Cervello@ivirma.com (I. Cervelló).
[1] FMJ and IC: equal contributing authors.

https://doi.org/10.1016/j.actbio.2019.03.004
1742-7061/

matrix (ECM) as an *in vitro* substratum. It is postulated that these complex mixtures aid to maintain functional characteristics of cells [1,2]. The ECM is a dynamic and complex milieu with biophysical, mechanical and biochemical properties and plays an important role in cell growth, development, homeostasis, regulation, and maturation [3]. In the female reproductive tract, the endometrial surface is a complex mixture of glycosaminoglycans, proteoglycans and fibrous structural proteins that interact with the embryo. Relatively few experiments have been done examining the physical requirements of pre-implantation embryos and the specific role of novel culture surfaces in embryo development within the laboratory, where inert surfaces such as polystyrene, glass and polydimethylsiloxane (PDMS) are used generally [4–9]. Thus, biologically derived coatings recapitulating and mimicking the original tissue composition could offer a promising approach for cell culture and embryo development in reproductive medicine [10].

Tissue engineering is a promising multidisciplinary field of investigation within regenerative medicine, poised to transform both translational medicine and investigation by designing materials resembling the structure and composition of native organs and tissues. This is also true for reproductive medicine, where reproductive tissue engineering or "REPROTEN" [11] is an interesting avenue to treat several pathologies leading to reproductive dysfunction (Mayer–Rokitansky–Küster–Hauser-syndrome, Asherman's syndrome and endometrial atrophy for example), for *in vitro* investigation and improving current *in vitro* Fertilization (IVF) advances. Several biomaterials have been proposed for these purposes, these can be synthetic [12,13], naturally derived polymers [14,15] or decellularized tissues [16–18]. Moreover, whole organ decellularization (DC) protocols have been successfully developed as possible new tool for transplantation technologies [19]. This has been done for virtually all major vital organs such as the lung [20], kidney [21], liver [22], heart [23], but also for murine and porcine uteri [17,18,24]. Related to reproduction, murine models showed that (acellular or recellularized) patches of these uterine bioscaffolds can improve regeneration and support gestation in a severe uterine horn damage model, demonstrating the value of decellularized tissues [18,25,26].

However, a decellularized organs' usability is not only limited to this, the complex mixture of extracellular proteins forming the tissue-specific ECM can be processed in various ways to serve different purposes [27]. For instance, sections or blocks of decellularized tissues can be made and seeded with primary culture cells, progenitor cells or endometrial stem (Side Population, SP, [28]) cells to create 3D cell culture systems [1,24,29]. Moreover, lyophilized, powdered tissue-specific ECM can be processed even further by digesting it into a liquid, with the objective to form a hydrogel or to coat a substrate. Hydrogels (synthetic or biological) are composed out of an insoluble 3D network of cross-linked hydrophilic polymers that have excellent biocompatibility, can encapsulate cells and are injectable before gel formation. For this versatility they are viewed as highly promising biomaterials for tissue engineering, regenerative medicine, and drug delivery applications [30]. By coating materials, you lose the native 3D architecture but load the conventional 2D environment with specific biochemical cues in a very reproducible manner. These biomaterial derived coatings have been developed from heart [31], liver [32], skeletal muscle [10], adipose tissue [33], central nervous system [34] but never for the endometrium. These studies showed that *in vitro* culture on these coatings improved cell differentiation and maturation into their respective tissue-specific cell fate. These biomimetic *in vitro* approaches would be also helpful to understand cellular and embryo development in the reproductive field.

By building on previous experience [24] we present here, to the best of our knowledge, the first study describing the DC of the rabbit uterus, where both non-proliferating (non-synchronous, NS) and proliferating (synchronous with the embryo, S) acellular endometrium were converted into a soluble form. This solubilized tissue-specific ECM formed stable and sterile hydrogels with a particular nanofibrous structure and was used as a novel biological coating for *in vitro* embryo culture. In this study, day 3 pre-implantation embryos were cultured on NS and S coatings and compared to various culture conditions.

The main objective was to demonstrate that specific ECM derived from synchronous decellularized endometrial rabbit tissues from uteri under ovarian hormone stimulation can produce an optimal substratum to improve *in vitro* culture. This investigation can prove to be valuable not only to innovate current human and non-human embryo culture but also to become an easily manageable platform for cell culture, *in vitro* drug screening and treatment of endometrial pathologies.

2. Material and methods

2.1. Study design

Four whole uteri were first decellularized, two of which were from non-synchronous rabbits having a non-proliferating endometrium and two from rabbits 72 h after ovarian stimulation (synchronous). After testing the DC efficiency, the acellular endometrium was separated via microdissection, lyophilized and milled. This powder enriched with complex ECM proteins was put into suspension by partial digestion, the pre-gel solution was aliquoted, stored at −80 °C and the resulting hydrogel was characterized (proteomics, electron microscopy, gelling kinetics). The biological function was tested by culturing day 3 embryos for 48 h in 5 different culture conditions: on three different biological surface coatings made from non-synchronous acellular endometrium (NS), synchronous acellular endometrium (S) and Matrigel (M) and in two standard culture conditions using uncoated wells with culture medium supplemented with and without 10% Fetal Bovine Serum (C + FBS and C−FBS, respectively). Hatching rates, morphometry and mRNA expression of 3 core pluripotency markers (*OCT4*, *Nanog* and *SOX2*) were analyzed and compared. A complete overview of the methodology is given in Fig. 1.

2.2. Animal setting

All the experimental procedures used in this study were performed in accordance with Directive 2010/63/EU EEC for animal experiments and were reviewed and approved by the Ethical Committee for Experimentation with Animals of the Universitat Politècnica de València, Spain (research code: 2018/VSC/PEA/0116). New Zealand White rabbits, an experimental animal in genetics and reproduction physiology since the beginning of the century, were used [35]. A major advantage of rabbit model is that it is one of the few species in which ovulation is induced by mating, resulting in an exactly defined pregnancy and embryonic age (hours or days post coitum) [35].

2.3. Whole uterus decellularization

Non-synchronous (NS) uterus (n = 2) were obtained from nulliparous rabbits, in which ovulation was not induced. For the synchronous (S) uterus (n = 2), ovulation was induced 72 h before extracting the uterus using hormonal treatment with 1 μg of Buserelin acetate (Hoechst Marion Roussel S.A., Madrid, Spain). To cannulate both uterine arteries, rabbits were euthanized with an intravenous injection of 200 mg/kg of pentobarbital sodium.

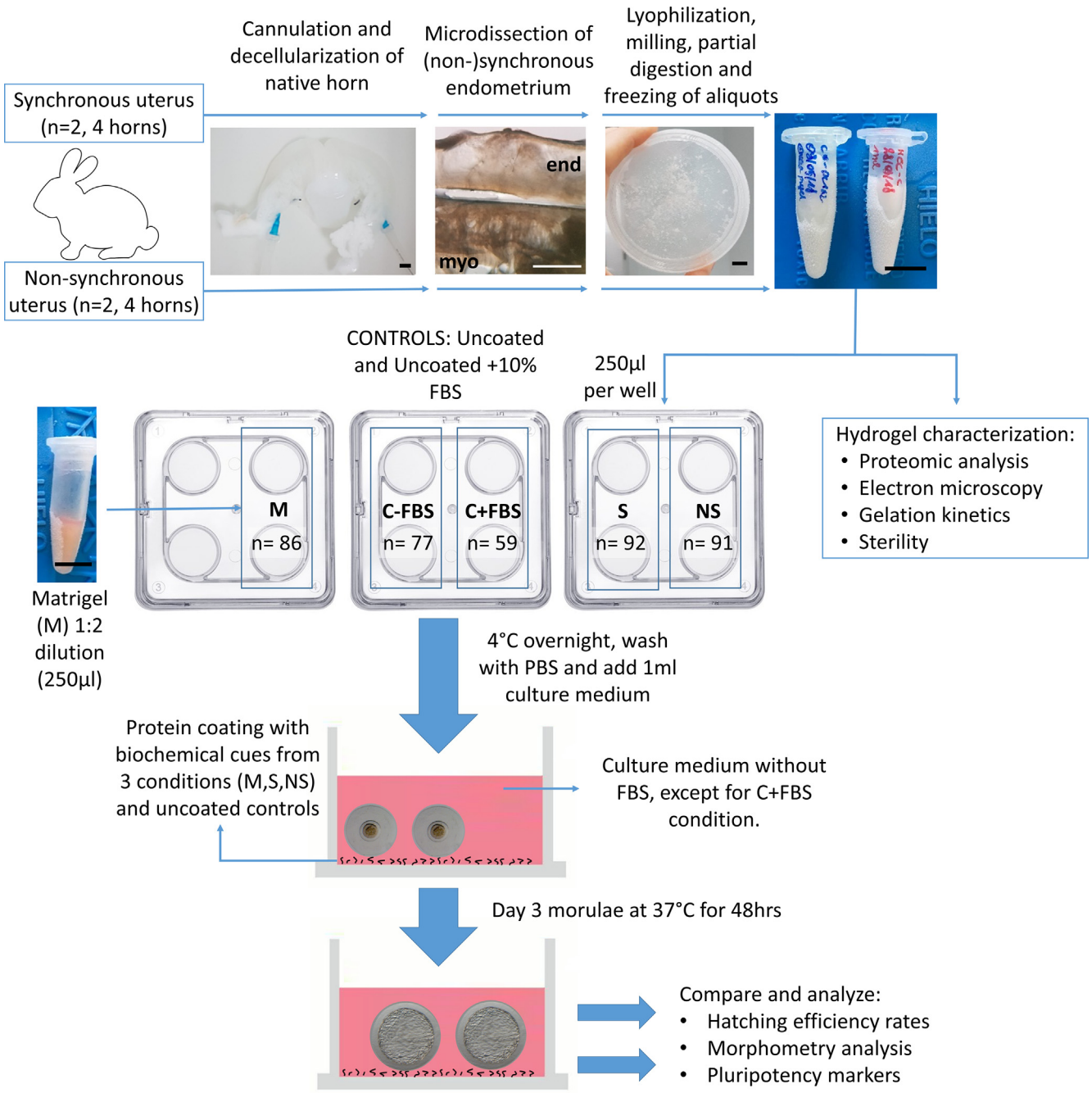

Fig. 1. Overview of experimental workflow. In total five different culture conditions (NS, S, M, C−FBS, C + FBS) were selected to culture day 3 embryos. Black and white scale bars are 1 cm and 0.1 cm respectively. Abbreviations: end: endometrium; FBS: fetal bovine serum; M: Matrigel; myo: myometrium NS: non-synchronous; S: synchronous. (For interpretation of the references to color in this figure legend, the reader is referred to the web version of this article.)

The uterine horns were flushed with PBS and EDTA (Sigma-Aldrich) to prevent clotting.

To decellularize both uterine rabbit horns the cannulated uterus was carefully attached to a peristaltic pump (Cole-Parmer instruments, Chicago, USA) using L/S 16 tubing (Masterflex, Fisher scientific). A protocol for the DC of pig uterus was first used for this study [24]. However, some modifications were made to be able to improve the removal of residual DNA in the rabbit model. This was done by perfusing during the last cycle with a 2 µg/mL DNase 1 solution (D4513-1VL), diluted in 1,3 mM MgSO4 and 2 mM CaCl2 (Sigma-Aldrich) for one hour. Table 1 shows the complete two-day protocol with the adaptations for the rabbit uterus, perfusion speed was set at 8 mL/min per horn.

2.4. Histological analysis

Circular segments from decellularized horns and native tissue were fixed overnight with 4% paraformaldehyde (PFA, Sigma-Aldrich) at 4 °C for histological analysis. They were dehydrated in graded alcohol/xylene baths and embedded in paraffin wax before being serially sectioned on a microtome (4 µm, HM 310, Microm) and mounted onto glass slides (Superfrost plus, Thermo Scientific). To assess the DC efficiency and ECM architecture, hematoxylin and eosin (H&E) and Masson's Trichrome (MT) stainings were used. To detect nuclear DNA, mounting media containing 6-diamidino-2-phenylindole (DAPI, Thermo-fisher Scientific) was used. All images were taken with a Nikon eclipse 80i microscope.

Table 1
Decellularization protocol for whole rabbit uteri. Abbreviations: PBS: phosphate buffered saline; H2Od: distilled water; SDS: sodium dodecyl sulfate.

	Reagent	Concentration	Duration
Cycle 1	PBS	1X	1 h
	SDS	0,1%	18 h
	H_2Od	–	30 min
	Triton-X100	1%	30 min
	PBS	1X	5 h
Cycle 2	SDS	0,1%	18 h
	H_2Od	–	30 min
	Triton X-100	1%	1 h
	PBS	1X	1 h
	DNase I solution	2 μg/mL	1h
	PBS	1X	3-4 h

2.5. Assessment of decellularization efficiency: DNA and protein quantification

The quantifications described below were done with the decellularized and control tissues. DNA was extracted from cubic pieces weighing <25 mg using a commercial kit (DNeasy Blood & Tissue, Qiagen), following the manufacturers protocol. DNA concentration was measured using the Qubit™ dsDNA HS Assay Kit (Thermo-fisher Scientific).

For protein quantification, pieces weighing around 0.1 g were minced and incubated with 100 μL of a modified Laemli buffer (0.125 M TrisHCl, 4% SDS, 10% β-mercaptoethanol, (Sigma-Aldrich)) for 48 h at 37 °C under agitation, protein concentration was determined using the Qubit Protein Assay Kit (Thermo-fisher Scientific).

2.6. Preparation of non-synchronous and synchronous acellular solubilized endometrial matrix for gelation and coating

From the decellularized and native (original/untreated) horn, 1 mm thick circular cuts put under a stereomicroscope (SMZ800, Nikon) and pure endometrial tissue was removed by cutting at the luminal side of the myometrium. Endometrial and myometrial fractions were washed a total of 4 times in ice cold PBS to remove enough residual SDS to have no measurable concentration when converted to hydrogels and stored at −80 °C. The endometrial fraction was lyophilized (Lyoquest-85, Telstar) overnight at 20 Pa and −80 °C and milled with dry ice in an ultra-centrifugal mill (ZM 200, Retch). The resulting powder was frozen a final time in liquid nitrogen, grinded by mortar and pestle and stored at −20 °C.

The decellularized endometrial powder was solubilized using a modified protocol [36]. Here, 1% (w/v) powder was suspended in 0.01 M HCl (Sigma-Aldrich) with 0.1% (w/v) of pepsin (Sigma-Aldrich), and left to digest for 48 h under constant agitation using a sterilized magnetic stirrer. Afterwards, the solution was left on ice and neutralized with 10% (v/v) 0.1 M NaOH (Sigma-Aldrich), and 11.11% (v/v) 10X PBS. The resulting solution was aliquoted, flash frozen in liquid nitrogen and stored at −80 °C.

To coat 4-well Nunc plates (Thermo-fisher Scientific), 250 μL of each solution (non-synchronous/NS, synchronous/S and 1:2 diluted Matrigel/M) was added and left overnight at 4 °C to let the proteins adhere nonspecifically. The coating solution was aspirated and wells were rinsed once with PBS before adding the culture medium.

2.7. Proteomic analysis

Tissue specific hydrogel (NS and S) solutions were diluted (1:1) with MilliQ water and the protein concentration in the new solutions was estimated by absorbance at 280 nm in a Nanodrop (Thermo Scientific). Then, 50 μg of every sample was loaded and resolved in a 1D SDS-PAGE gel. Every sample lane was sliced in 7 equivalents fragments. Gel slides were digested using 200 ng of sequencing grade trypsin (Promega) as described elsewhere [37]. The trypsin digestion was stopped with 10% trifluoroacetic acid (TFA) and the supernatant (SN) was removed, then the library gel slides were dehydrated with pure acetonitrile (ACN). The new peptide solutions were combined with the corresponding SN. The peptide mixtures were dried in a speed vacuum and resuspended in 2% ACN; 0.1% TFA. The final volume was 10 μL.

Liquid chromatography and tandem mass spectrometry (LC–MS/MS) was performed, proteins showing unused score >1.3 were identified with confidence ≥95% and bioinformatics analysis of proteomics profiles were carried out. Mass spectrometry information of all the fragments were combined for protein identification. Here, ProteinPilot default parameters were used to generate peak list directly from 5600 TripleTof wiff files. The Paragon algorithm [38] of ProteinPilot v 5.0 was used to search the UniprotMammals database (version 03-2018) with the following parameters: Trypsin specificity, (iodoacetamide) cys-alkylation, taxonomy not restricted, and the search effort set to through. The protein grouping was done by Pro group algorithm. Here, the formation of protein groups is guided entirely by observed peptides only, which originate from the experimentally acquired spectra. Because of this, the grouping can be considered to be guided by usage of spectra.

The proteomic analysis was performed in the proteomics facility of SCSIE University of Valencia.

2.8. Hydrogel characterization: Fiber size, gelation kinetics and sterility

To analyze the fiber size and density scanning electron microscopy (SEM) was used; they were fixed in 2,5% glutaraldehyde in PBS (Sigma Aldrich, Grade II, 25%) and then slowly critical point dried, coated with gold-palladium for 2 min using a SC7640 Sputter Coater (Quorum technologies) and imaged with a SEM FEG Hitachi S-4800. Fiber diameter was measured using ImageJ software.

The gelation kinetics (n = 4 and n = 3 for S and NS hydrogel respectively) were evaluated by turbidimetry, 100 μL of each solution was added in 96-well plates and absorbance was measured at 405 nm every minute. Values were normalized by the following formula taken from Wolf et al. [39]: $NA = \frac{A-A_0}{A_{max}-A_0}$ (NA: normalized absorbance, A: measurement at given time, A0: absorbance at t = 0 m, A_{max}: maximum absorbance). The lag time (time before turbidity increases) and time to reach 50% of the maximal absorbance were calculated.

To test structural stability and sterility, gels (NS, S and M) were left in DMEM/F12 medium containing 10% FBS and 0.1% antibiotics for 7 days.

2.9. Biological properties and applications of hydrogels

To assess the biological activity of the pregel solution, we perform an *in vitro* embryo culture test, where late stage morulae/early stage blastocyst are cultured on 3 different coatings (NS, S, M) in culture medium without FBS evaluating its hatching/hatched rate (Supplementary Fig. 1), degree of expansion and the expression of the three core pluripotency factors (*OCT4*, *Nanog* and *SOX2*).

Twelve New Zealand White rabbits were used as embryo donors. Ovarian stimulation was induced using 3 μg of Corifollitropin alfa (Elonva, Merck Sharp & Dohme S.A.; Spain) with 10% of recombinant human LH (Luveris 75; Serono Europe Ltd., London, United Kingdom) [40]. Ovulation was induced using 1 μg of buserelin acetate (Hoechst Marion Roussel S.A., Madrid, Spain)

and artificial insemination was done using a heterospermic pool of semen from male animals of the same line to randomize male effect. After 72 h, morphologically higher quality embryos (late morulae and early blastocysts) classified as excellent (presenting homogenous cellular mass, mucin coat and spherical zona pellucida according to the International Embryo Technology Soc) were pooled to randomize donor effect. Then, embryos were cultured for 48 h in Tissue Culture Medium 199 (TCM199 (Sigma-Aldrich) with antibiotics) at 38.5 °C, 5% CO_2 and saturated humidity. The *in vitro* development ability of embryos was assessed based on the hatching/hatched rate (proportion of hatching and hatched blastocyst at 48 h of culture from total cultured embryos). The hatched state was achieved when >50% of the embryonic mass cell was extruded of zona pellucida.

For the morphometric analysis digital images of hatched blastocysts were taken using a Nikon optical microscope from 43, 43, 22, 41 and 48 embryos cultured in C−FBS, C + FBS, M, NS and S experimental groups, respectively. For each embryo, the maximum and minimum distance of an adjusted oval section drawn around the embryo were used to calculate the mean diameter value in the maximal cross-sectional image. Pictures were analyzed using the ImageJ program after calibration with a graduated ruler (Supplementary Fig. 2).

Finally, the gene expression profile of the three core pluripotency factors (*OCT4*, *Nanog* and *SOX2*) was assessed after the 48 h of *in vitro* culture. From each embryo culture batches, all embryos were used to mRNA expression determination. Total RNA was extracted using the Dynabeads kit (Life Technologies, Carlsbad, CA, USA), following the manufacturer's instructions. Then, reverse transcription was carried out using qScript^{TM}cDNA Synthesis kit (Quanta Biosciences, Beverly, MA, USA) following the manufacturer's instructions. Real time PCR reactions were performed in an Applied Biosystems 7500 system (Applied Biosystems). Every PCR was performed from 5 μL diluted 1:10 complementary DNA (cDNA) template, 250-nM of forward and reverse specific primers (Table 2), and 15 μL of Power SYBR Green PCR Master Mix (Fermentas Gmbh, Madrid, Spain) in a final volume of 20 μL. Relative gene expression was calculated via ΔΔCt method adjusted for PCR efficiency, applying the geometric average of the glyceraldehyde-3-phosphate dehydrogenase (*GAPDH*) and the H2A histone family member Z (*H2AFZ*) housekeeping genes as normalization factor [41].

2.10. Statistical analysis

To identify any significant differences of DNA and protein levels before and after DC ANOVA was first used. If the means of the three populations were not considered as equal, we followed up with a posthoc test (Bonferroni method). A P-value obtained in a two-tailed test $\leq$0.05 was considered statistically significant.

A general linear model was fitted for the analysis *in vitro* development rate, including as fixed effect the experimental group with five levels (NS, S, M, C−FBS, C + FBS). Development rate were computed as the difference in their least squares means ± standard error of means.

Differences in the morphometric and gene expression between the experimental groups (NS, S, M, C−FBS and C + FBS) were estimated using Bayesian inference. Bounded flat priors were used for all unknowns and the marginal posterior distributions were estimated by Gibbs sampling. Both descriptive statistics and phenotypic differences were computed with the program Rabbit developed by the Institute for Animal Science and Technology (Valencia, Spain). After some exploratory analyses, results were based on Markov chain Monte Carlo chains consisting of 60.000 iterations, with a burn-in period of 10.000, and saving only 1 of every 10 samples for inferences. Summary statistics from the marginal posterior distributions were calculated directly from the samples saved. In all analyses, convergence was tested using the Z criterion of Geweke. The parameters obtained from the marginal posterior distributions of the differences between experimental groups were the mean of the difference between the experimental groups, the highest posterior density region at 95% of probability ($HPD_{95\%}$) and the probability (P) of the difference being >0 when $D_{CP\text{-}VP} > 0$ or lower than 0 when $D_{CP\text{-}VP} < 0$ (Supplementary Tables 1 and 2). Differences were considered relevant if $P \geq 0.8$ (80%). A more detailed description of these features can be found in Blasco [42].

3. Results

3.1. Macroscopical, histological and quantitative analysis of rabbit uteri decellularization

Visually, both horns of the uterus (n = 4, 8 horns) turned white/opaque after the DC protocol, with no meaningful differences between non-synchronous (NS) and synchronous (S) uteri, nor within the replications (Fig. 2A and B). Rabbit uteri described as NS and S correspond respectively to hormonally (un)treated animals as described previously. DC was first verified by histological methods: H&E and Masson's trichrome staining showed the complete removal of cellular material and nuclei in all layers while preserving the ECM architecture, consisting predominantly out of collagens (Fig. 2A1-2 and B1-2). Representative images of the histology were used. Furthermore, DAPI staining confirmed the complete destruction of the nuclei in all uterine layers (Fig. 2A3 and B3). This was corroborated by the quantification of the residual DNA, a significant reduction ($P < 0.001$) compared to the native uterus was measured for both NS and S uterus (220 ± 50 vs 10 ± 4 and 15 ± 8 ng DNA per mg wet tissue respectively, Fig. 2C). Similarly, protein content significantly ($P < 0.05$) dropped from 20 ± 3 to 11 ± 3 and 12 ± 5 μg proteins per mg wet tissue respectively (Fig. 2D). No difference in histology (not shown) or quantification ($P < 0.05$) was observed between both types of uterus.

3.2. Microdissection of decellularized endometrial tissue

When the thin circular cuts were placed under a stereomicroscope, a transparent layer became apparent in the native tissue, the elongated fibrous ECM of the myometrium are also apparent in the decellularized tissue (Fig. 3A and C). This ribbon appears because the rabbit myometrium consists of an inner circular and

Table 2
List of primers used for quantitative real-time PCR. Abbreviations: OCT4: transcription factor octamer-binding 4; NANOG: NANOG homeobox; SOX2: sex-determining region Y-box 2; H2AFZ: H2A histone family member Z; GAPDH: glyceraldehyde-3-phosphate dehydrogenase.

Gene symbol	Forward primer	Reverse primer	Fragment (bp)
OCT4	CGAGTGAGAGGCAACTTGG	CGGTTACAGAACCACACACG	125
NANOG	CCAGGTGCCTCTTACAGACA	TCACTACTCTGGGACTGGGA	104
SOX2	AGCATGATGCAGGAGCAG	GGAGTGGGAGGAAGAGGT	270
H2AFZ	AGAGCCGGCTGCCAGTTCC	CAGTCGCGCCCACACGTCC	85
GAPDH	GCCGCTTCTTCTCGTGCAG	ATGGATCATTGATGGCGACAACAT	144

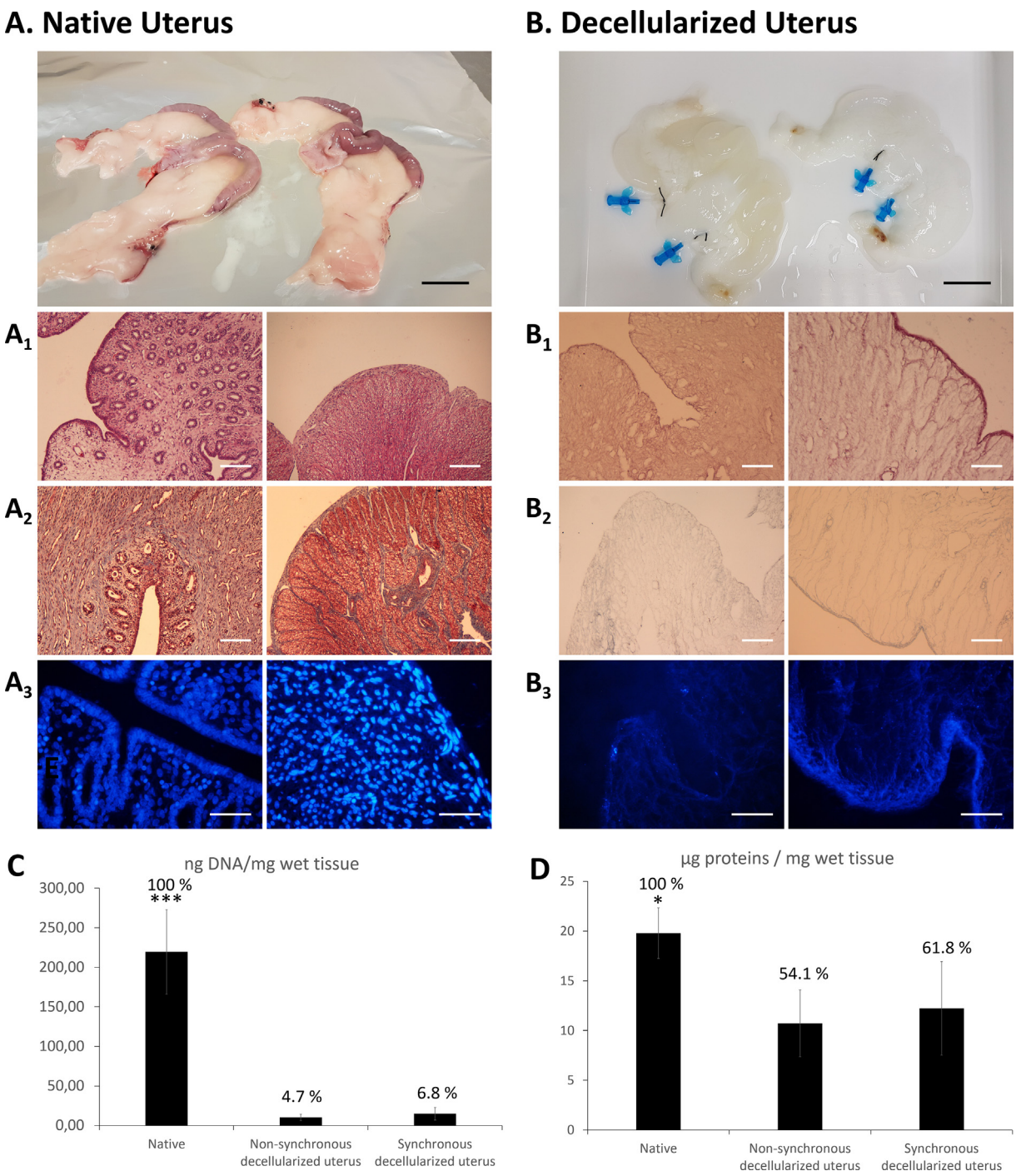

Fig. 2. Decellularization of rabbit uterus. Macroscopic aspect of rabbit uteri before (A) and after (B) decellularization, blood and cellular material was lysed and removed via perfusion resulting in an opaque/white organ. (A&B) Representative histological images of native and decellularized endometrium (left) and myo-perimetrium (right) demonstrating full DC throughout the uterus. H&E (A_1 & B_1) and Masson's trichrome stain (A_2 & B_2) demonstrate removal of cellular material and an intact ECM rich in collagens. Scale bars are 150 µm. (A_3 & B_3) DAPI stain showing complete destruction of nuclei though all layers. Scale bars are 50 µm. (C) DNA quantification with Qubit™ dsDNA HS Assay confirmed a 95.3% and 93.2% reduction in double stranded DNA for the non-synchronous and synchronous decellularized uterus respectively. (D) Qubit Protein Assay Kit showed a 45.9% and 38.2% decrease in protein concentration in both tissues. *** and * denote significance from all other data points as indicated by an ANOVA with Bonferroni correction (***$p < 0.001$ and *$p < 0.05$). (For interpretation of the references to color in this figure legend, the reader is referred to the web version of this article.)

outer longitudinal smooth muscle layer, and by making circular cuts we aligned the correct muscle fibers and could use it as separation guide. After opening the uterine horn, the endometrium was cut at the luminal side of the myometrium (Fig. 3A and C). To verify the endometrial purity, a collection of separated endo- and myometrium of the native tissue were stained by H&E (Fig. 3B). Here it is apparent that the incisions are being made above the muscle layer, in the endometrium, resulting a pure tissue (typical stromal and epithelial glandular structures) for both native and decellularized tissue.

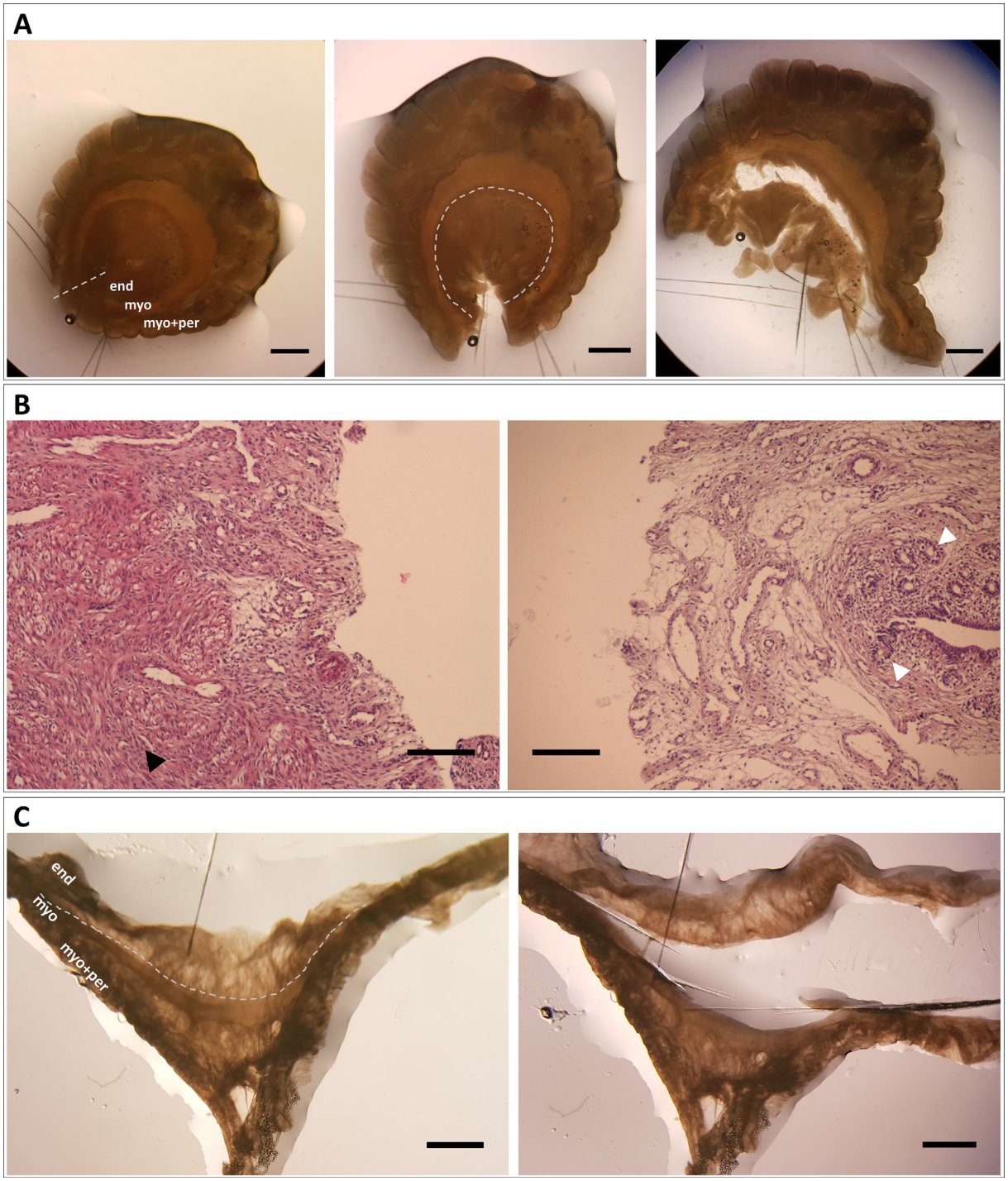

Fig. 3. Microdissection of uterine tissues. (A) Separation of endometrium in native tissue as proof-of-concept, the 3 prominent layers are apparent (end: endometrium, myo: inner myometrium, myo + per: outer myometrium + perimetrium), in total 2 cuts are being made as shown by the dotted line, one to open the uterine horn (left) and the other one where cuts are being made at the luminal side of the myometrial layer (middle). Scale bars are 0.2 cm. (B) Representative images of H&E stain of separated native myometrium (left) and endometrium (right), black arrow head showing the inner circular smooth muscle layer, white arrow heads howing gland of non-synchronous endometrium. Scale bars are 150 μm. (C) Separation of decellularized tissue, the aligned ECM from the myometrial cells is distinguishable (myo) and cuts were made following the dotted line. Scale bars are 0.2 cm. (For interpretation of the references to color in this figure legend, the reader is referred to the web version of this article.)

3.3. Hydrogel preparation and biochemical properties

The lyophilized non-synchronous (NS) and synchronous (S) acellular endometrium were milled until a grain size smaller than 0, 0625 mm^2 in a ultracentrifugal mill, this powder was put into suspension until no more tissue was visible (Supplementary Fig. 3A–C). The resulting viscous pre-gel solutions formed stable hydrogels that required gentle handling when left at 37 °C for one hour (Supplementary Fig. 3D). Long-term structural stability and sterility of this ECM derived gel was demonstrated by incubating them at 37 °C in standard cell culture medium for 7 days. The hydrogel remained intact during this period and no bacterial growth was observed (Supplementary Fig. 3E). Both hydrogels were subjected to a qualitative proteomic analysis to evaluate their

protein composition (Fig. 4A). Based on previous work describing this kind of analysis we decided to exclude undesirable contaminants originating from the laboratory such as keratin and uncharacterized proteins for our analysis and focus on the growth factors and ECM proteins [43]. Here, no meaningful differences between both types of hydrogels were observed. Both hydrogels had a composition rich in fibrillin, collagens and laminin, furthermore some growth factors were measured. Fig. 4A shows the average ratio of these components and can be considered as the general composition of these endometrial hydrogels, surprisingly a high percentage (40.73%) of fibrillin was observed, followed by collagens (36.79%) and laminin (13.32%). Trace amounts of growth factors (fibroblast growth factor, norrin cystine knot growth factor, transforming growth factor) were also measured. When comparing the basement membrane components of both types it appears that laminins are better retained in the S gel (Fig. 4B). There was also a higher relative abundance of basement membrane proteins in the S gel (not shown). Further analysis shows that laminin subunit beta 1 is better preserved in the S hydrogel but no other large differences were observed in the composition of other main ECM components (Supplementary Fig. 4).

3.4. Hydrogel characterization: Gelling kinetics and ultrastructure

Both hydrogels were subjected to turbidimetric analysis, for which gelation kinetics were measured spectrophotometrically and several parameters were calculated (t_{lag} and $t_{1/2}$). Both gelation kinetics followed a sigmoidal curve, but significant differences were observed in the $t_{1/2}$ parameters (Supplementary Fig. 5). Gelation of the S hydrogel started earlier tended to have a lower lag time than the NS hydrogel (t_{lag} = 3.0 ± 0.9 min vs 4.9 ± 0.3 min). The time to reach 50% of the maximal gelation did show significant differences, where the S gel needed about 5 min less than the NS hydrogel ($t_{1/2}$ = 10.4 ± 0.7 min and 15.5 ± 0.3 min respectively, Supplementary Fig. 5).

Even though the hydrogels lost their original ECM organization, SEM of the gel surface showed that both NS and S gels have a homogenous, randomly interlocking fibrillar structure of similar density (Fig. 5A and B). Fiber diameter of the NS and S hydrogel was analyzed from images taken at 60.000× resolution (>30 measurements per hydrogel, Fig. 5C–F). The diameter of the reassembled nanofibers from both gels range between 50 and 149 nm, measuring on average 70 ± 9 vs 100 ± 20 for the NS and S hydrogel respectively. A significant difference ($P < 0.05$) between both fiber diameters was found. It is possible that the collagen fibrils, having a thickness of 50 nm on average remained more bundled in the S hydrogel, or that components interacting with the fibers persisted. It is also apparent that the majority of fibers of the NS and S gels show the D-periodicity typical for collagen fibrils, in contrast to the Matrigel hydrogel (Fig. 5C–F).

3.5. Effect of endometrial coatings on in vitro embryo development and mRNA expression

In vitro development was not significantly affected by culture conditions, the mean value of hatching rates was 89 ± 3%. The

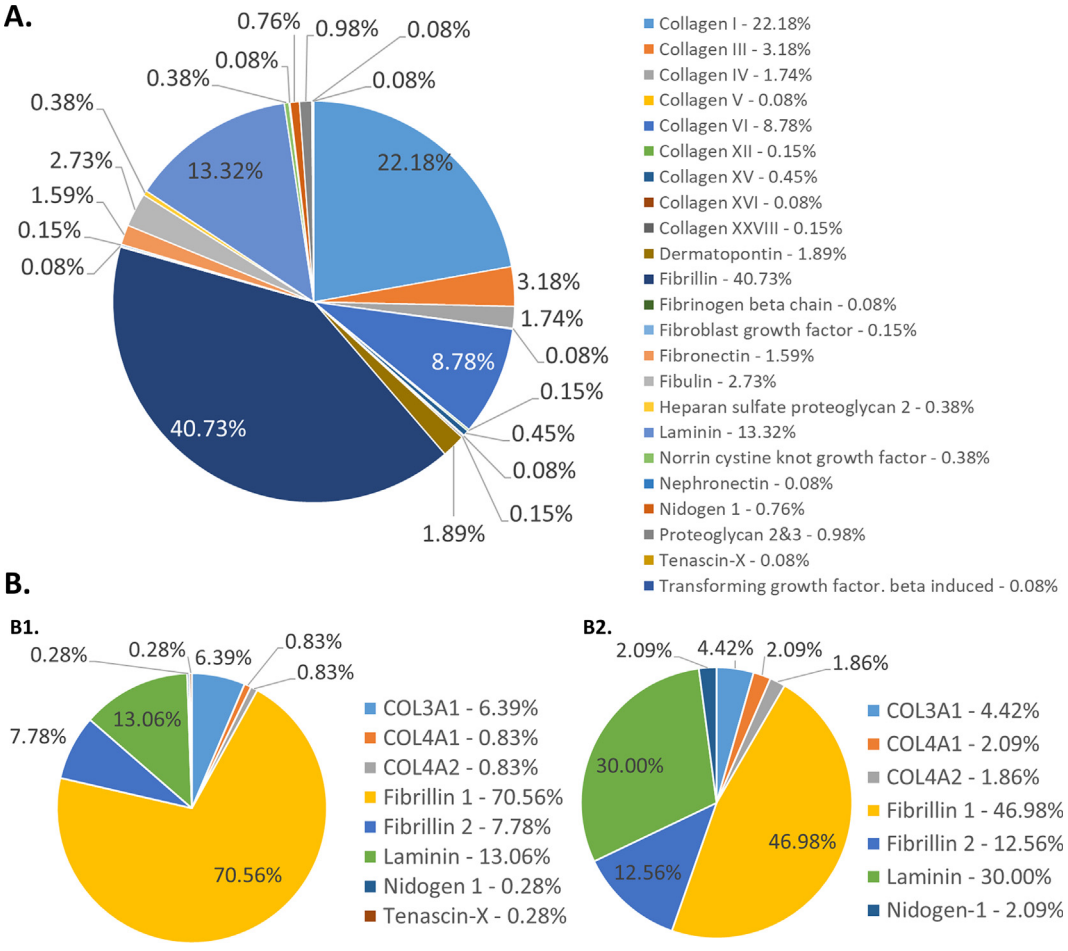

Fig. 4. Quantitative assessment of ECM protein composition of hydrogels by liquid chromatography-tandem mass spectrometry. (A) Combined relative percentage of ECM proteins in non-synchronous and synchronous endometrial hydrogel. (B) Relative percentage of basement membrane components in non-synchronous (B1) and synchronous (B2) hydrogel.

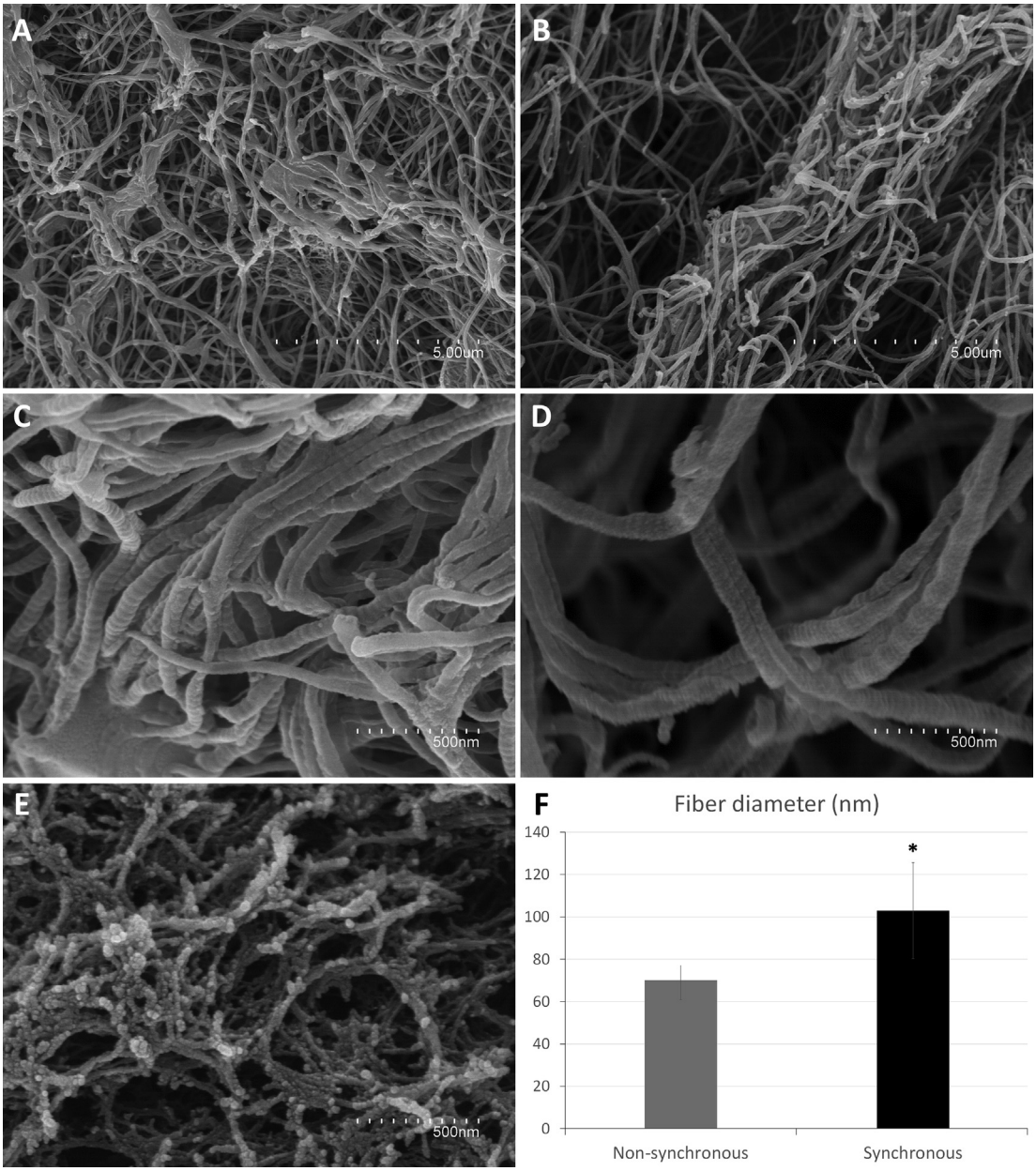

Fig. 5. Ultrastructure of endometrial ECM hydrogels. Representative scanning electron micrographs at 10.000× magnification of ultrastructure of non-synchronous (A) and synchronous (B) gel with nanofibers ranging between approximately 50 and 150 nm thick and showing similar density. Scale bars are 5 μm. Fibers were evaluated and measured using micrographs at 60.000× magnification of non-synchronous (C), synchronous (D) hydrogel and Matrigel (E), showing their characteristic morphologies such as D-periodicity for the ECM hydrogels. These and similar images were used to measure the diameter with ImageJ software. Scale bars are 500 nm. (F) The average diameter of both ECM hydrogels shows a significant difference. The differences of fiber diameter between NS and S gels were calculated with a significance level = $^{*}p < 0.05$.

mean diameter of the embryos of S and C + FBS groups was significantly higher than the diameter of the NS, C-FBS and M groups after 48 h of *in vitro* culture (Fig. 6A). In addition, the pattern of mRNA expression of *NANOG* was not significantly affected by culture conditions. Nevertheless, embryos developed in NS gels group showed higher levels of *OCT4* transcript abundance than C−FBS group, while *SOX2* transcript abundance was higher in the blastocysts developed in NS gel, S gel and C + FBS groups, in comparison with the Matrigel and C−FBS groups (Fig. 6B).

4. Discussion

Ever since its first publication over 20 years ago [44], the DC and solubilization of tissues and organs has been rising in popularity and has been applied to all important organ systems [45]. To the best of our knowledge, this has never been done before for the endometrium. In this context, a dual hypothesis was formulated. First, that a biologically native ECM derived from endometrial decellularized tissues renders more a physiologically suitable microenvironment for *in vitro* culture techniques. Secondly, that the drastic cyclical changes within the endometrium are translated to these substrata, and that this is noticeable in *in vitro* embryo culture. In this study, we demonstrate that the specificity of NS and S endometrium remains after a gentle SDS-based DC protocol and treatment with pepsin to convert it into a pre-gel solution. Here we present one of the first studies using this novel type of biomaterials made from reproductive tissues [46].

Based on earlier successful results in the pig model we slightly adapted the protocol using SDS and Triton X-100 for the rabbit

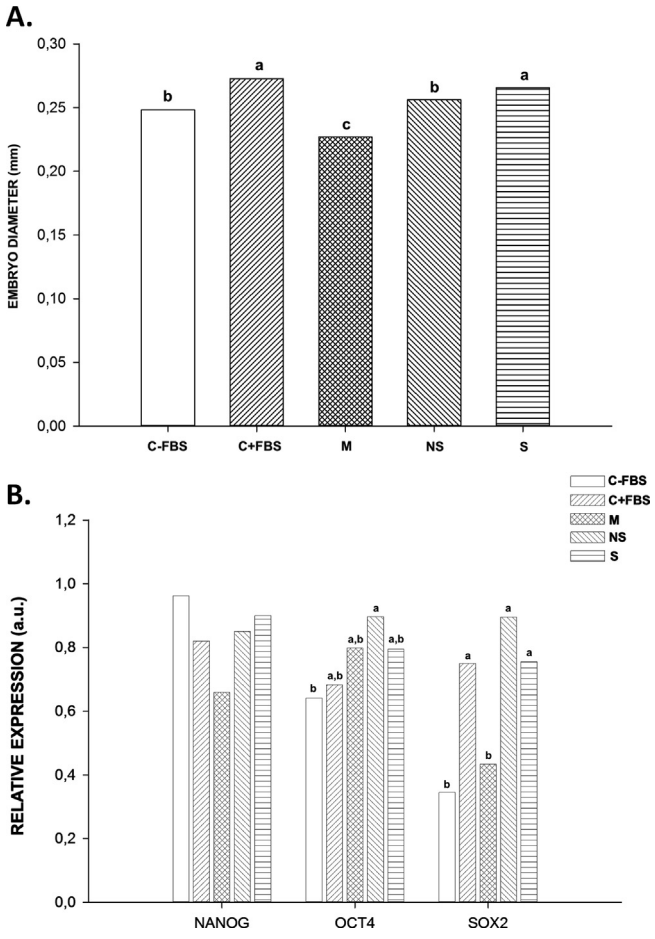

Fig. 6. Effect of different biological surface coatings on embryo diameter and mRNA transcription levels of core pluripotency markers. Diameter and transcription values are expressed as the mean value for each condition. a–c: Data with uncommon letters are different. Differences were considered if the probability of the difference between groups was ≥0.8 (80%) using Bayesian inference methods. (A) These coatings were made from non-synchronous acellular endometrium (NS), synchronous acellular endometrium (S) and Matrigel (M) and two standard culture conditions using uncoated wells with culture medium supplemented with and without 10% Fetal Bovine Serum (C + FBS and C−FBS, respectively) on embryo diameter after 48 h of *in vitro* culture, identical letters represent similar results. (B) *OCT4*, *SOX2* and *NANOG* levels were determined in embryos after 48 h *in vitro* culture on NS, S and M biological surface coatings and two standard culture conditions (C + FBS and C−FBS, respectively). Values from real-time PCR were normalized to geometric average of H2AFZ and GAPDH.

uterus [24]. These chemical components are commonly used and have demonstrated its effectiveness to create bioscaffolds from various tissues and organs that are implantable and can be recellularized. Histology showed that the general morphology of the NS and S uteri after DC was very similar; this was further corroborated by DNA quantification, where a sufficient reduction of approximately 95% in DNA content was observed. It is possible that the total DNA per dry weight exceeds that of previously established criteria [19] but the significance of this is still up for debate. For example, aortic root scaffolds with much higher DNA contents have shown no tissue rejection after transplantation [47], making it unlikely for this bioscaffold to elicit such response, especially after converting it into a less dense pre-gel solution. In addition, several studies using *in vitro* culture have demonstrated the inductive capacities and the beneficial effects of decellularized (and solubilized) tissues to guide the differentiation of stem cells [48] and to preserve the phenotype of primary cell culture [2]. The biochemical and biomechanical differences after DC are not only retained between different tissues, it has been shown that this also is the case within tissues, for example when suffering from certain pathologies such as fibrosis [49], amyloidosis [50,51] or cancer [52,53]. Even the age of the donor tissue has been shown to affect the *in vitro* culture of a 3D bioengineered model of cortical brain tissue [54]. In the reproductive field, under the influence of the female sex steroids, the endometrium undergoes cycles of drastic growth and reorganization in order to accept the embryo [55,56]. The ECM of the endometrial tissue follows this cycle with differential expression of both interstitial and basement membrane proteins, many of which remain after DC [57–60]. Even though DC also negatively affects the ECM, the main components and their differences can be appreciated after the proteomic analysis of both hydrogels. Furthermore, growth factors can be immobilized *in vivo* though glycosaminoglycans linked to ECM proteins [61]. Here we theorize that the complex mixture of ECM proteins and sequestered biochemical signals between a NS and S endometrium are distinct enough to see differences in the most sensitive *in vitro* model, namely the embryo development. After a quantitative analysis of the protein composition it is likely that the main differences observed *in vitro* are the result of sequestered growth factors and/or of certain ECM proteins. Basement membrane proteins such as laminin and collagen IV showed higher abundance in the hydrogel made of the proliferating endometrium (containing more glands). Interestingly, laminin has been described recently to promiscuously bind to growth factors with high affinity [62] and was found in higher relative concentrations in the S hydrogel. This would imply a higher potential of the synchronous substrata to retain important growth factors. When comparing to the nonspecific commercial coatings that most likely lack these components in these concentrations an impaired development was observed. Matrigel is a solubilized basement membrane solution extracted from Engelbreth-Holm-Swarm (EHS) mouse sarcoma and is unlikely to have any use in any clinical setting. The use of Matrigel and ECM component hyaluronic acid as supplement of culture medium and coating for embryo culture were investigated in the past but conflicting results were reported [4,5,8,63].

The separation of tissues from whole decellularized structures has been published recently by other groups [64], and comparable techniques were used to separate the acellular NS and S endometrium along our study. Circular tissue sections were tested initially but the poor transparency and difficult manipulation of the embryo for quality assessment and morphokinetic analysis made this option unviable. While only slight differences were observed between the hydrogels, this was not the case when comparing the gelling kinetics and ultrastructure of the NS and S hydrogel. Here, significantly thicker fibers are observed. It is known that cells start remodeling the absorbed ECM surface after the first interaction and that the cellular proteolytic activity increases when interfacing with a strongly bound ECM substratum and no serum in the culture medium is present [65]. The rabbit blastocyst has a fusion type implantation and does not invade the endometrium, nonetheless it has been shown that it also produces proteases [66]. When the coating was made from the synchronous endometrium (S group), the similar blastocyst hatching rates, size and pluripotency resembling those grown in standard positive conditions (using FBS), effectively compensating for the absence of adhesion proteins and growth factors of the serum in the culture medium. Our results showed a similar pattern in *OCT4* and *SOX2* expression in the synchronous endometrium and serum group. The Sox2-Oct4-Nanog regulatory complex controls expression of pluripotency genes through feed-forward loops [67] including these three genes in an autoregulatory circuit [68]. Perhaps, an inadequate mRNA expression might trigger failures in the development and implantation of the embryos. In line with this highlighting the important role of Sox2 in the preimplantation mouse embryo [69]. Thus, our

result seems to demonstrate that synchronous endometrium coating would retain and release compounds that permit in part mimic the endometrial environment under *in vitro* conditions. Here we clearly demonstrate that a tissue-specific coating is necessary to even approach or improve on serum free culture conditions and that the M coating has a distinct negative effect on the embryo.

Many possible future applications and investigations are possible using the flexibility of these ECM hydrogels and coatings. Coating synthetic implants *in vivo* modulates the host immune response, improving biocompatibility and subsequent recovery [70,71]. The most interesting aspect of these injectable pre-gel solutions for regenerative medicine is that they can be used as acellular scaffolds [72] or can be doped with stem cells [73] or growth factors [73,74] and can be used as possible non-invasive treatment for endometrial pathologies such as endometrial atrophy and Asherman's syndrome, improving on previous investigations using cell therapy [75]. A potential limitation concerning the clinical translation could be the animal origin of the ECM due to the potential for disease transmission and immunological reaction however the FDA has approved many decellularized tissue-specific ECM for human uses as porcine dermis, small intestine mucosa and heart valves [76] suggesting them as a viable option for *in vitro* techniques. Furthermore, an ECM hydrogel therapy for myocardial infarction is already in a Phase 1 clinical trial (ClinicalTrials.gov Identifier: NCT02305602).

Altogether, in this study we present that endometrial tissue-specific ECM derived coatings obtained from whole organ decellularized create a biomimetic environment allowing for the growth of pre-implantation embryos. Furthermore, this sensitive *in vitro* technique demonstrates that the specific mixture of biochemical signals derived from the native microenvironment is retained after biochemical and mechanical treatments. We strongly demonstrated the appropriate preservation of the ECM providing for the first time the initial step to mimic the endometrial environment *in vitro*. When the coating is from the endometrium synchronous with the developing blastocyst the expression and development of the embryo is improved compared to NS and M coatings and is the only condition comparable with the current gold standard. More investigation is still needed to fully demonstrate the possible uses of these hydrogels in applied research and reproductive medicine.

5. Conclusions

Tissue engineering is a promising and burgeoning multidisciplinary field of investigation, poised to transform translational medicine and investigation. Along this study, a DC protocol for whole rabbit uteri was established and endometrial ECM hydrogels were obtained. For the first time, we demonstrated that coatings from synchronous decellularized endometrium act as a biomimetic support for rabbit embryo development and is comparable to optimal protocols, possibly because of the slow release of synchronous-specific endometrial proteins. While more investigation is needed to improve upon current techniques, it is apparent that bioengineered tissue-specific approaches are a promising avenue to one day revolutionize reproductive medicine.

Acknowledgements

This study was supported by the following entities: GRISOLIA/2015/002 (HC); PI17/01039 (IC); Prometeo/2018/137 (IC); AGL2017-85162-C2-1-R; BES-2015-072429 (XGD); ACIF/2017/118 (SLM). The proteomics laboratory is a member of Proteored, PRB3 and is supported by grant PT17/0019, of the PE I + D + i 2013-2016, funded by ISCIII and ERDF.

Appendix A. Supplementary data

Supplementary data to this article can be found online at https://doi.org/10.1016/j.actbio.2019.03.004.

References

[1] S. Xiao, J.R. Coppeta, H.B. Rogers, B.C. Isenberg, J. Zhu, S.A. Olalekan, K.E. McKinnon, D. Dokic, A.S. Rashedi, D.J. Haisenleder, S.S. Malpani, C.A. Arnold-Murray, K. Chen, M. Jiang, L. Bai, C.T. Nguyen, J. Zhang, M.M. Laronda, T.J. Hope, K.P. Maniar, M.E. Pavone, M.J. Avram, E.C. Sefton, S. Getsios, J.E. Burdette, J.J. Kim, J.T. Borenstein, T.K. Woodruff, A microfluidic culture model of the human reproductive tract and 28-day menstrual cycle, Nat. Commun. 8 (2017) 14584.

[2] R. Lang, M.M. Stern, L. Smith, Y. Liu, S. Bharadwaj, G. Liu, P.M. Baptista, C.R. Bergman, S. Soker, J.J. Yoo, A. Atala, Y. Zhang, Three-dimensional culture of hepatocytes on porcine liver tissue-derived extracellular matrix, Biomaterials 32 (2011) 7042–7052, https://doi.org/10.1016/j.biomaterials.2011.06.005.

[3] H. Zhang, F. Tasnim, J.Y. Ying, D. Zink, The impact of extracellular matrix coatings on the performance of human renal cells applied in bioartificial kidneys, Biomaterials 30 (2009) 2899–2911, https://doi.org/10.1016/j.biomaterials.2009.01.046.

[4] K.M. Dawson, J.M. Baltz, P. Claman, Culture with Matrigel inhibits development of mouse zygotes, J. Assist. Reprod. Genet. 14 (1997) 543–548.

[5] L. Lazzaroni, F. Fusi, N. Doldi, A. Ferrari, The use of Matrigel∗ at low concentration enhances in vitro blastocyst formation and hatching in a mouse embryo model∗∗Matrigel, Becton Dickinson Labware, Bedford, Massachusetts, Fertil. Steril. 71 (1999) 1133–1137, https://doi.org/10.1016/S0015-0282(99)00149-1.

[6] F.R. Parikh, S.G. Nadkarni, N.J. Naik, D.J. Naik, S.A. Uttamchandani, Cumulus coculture and cumulus-aided embryo transfer increases pregnancy rates in patients undergoing in vitro fertilization, Fertil. Steril. 86 (2006) 839–847, https://doi.org/10.1016/j.fertnstert.2006.03.028.

[7] Y.L. Lee, J.S. Xu, S.T.H. Chan, P.C. Ho, W.S.B. Yeung, Animal experimentation: vero cells, but not oviductal cells, increase the hatching frequency and total cell count of mouse blastocysts partly by changing energy substrate concentrations in culture medium, J. Assist. Reprod. Genet. 18 (2001) 566–574, https://doi.org/10.1023/A:1011910125079.

[8] A.T. Palasz, H. Rodriguez-Martinez, P. Beltran-Breña, S. Perez-Garnelo, M.F. Martinez, A. Gutierrez-Adan, J. De la Fuente, Effects of hyaluronan, BSA, and serum on bovine embryo in vitro development, ultrastructure, and gene expression patterns, Mol. Reprod. Dev. 73 (2006) 1503–1511, https://doi.org/10.1002/mrd.20516.

[9] T.T. Peura, G. Vajta, A comparison of established and new approaches in ovine and bovine nuclear transfer, Clon. Stem Cells. 5 (2003) 257–277, https://doi.org/10.1089/153623003772032772.

[10] J.A. DeQuach, V. Mezzano, A. Miglani, S. Lange, G.M. Keller, F. Sheikh, K.L. Christman, Simple and high yielding method for preparing tissue specific extracellular matrix coatings for cell culture, PLoS One 5 (2010), https://doi.org/10.1371/journal.pone.0013039 e13039.

[11] C.A. Amorim, Special issue devoted to a new field of regenerative medicine: reproductive tissue engineering, Ann. Biomed. Eng. 45 (7) (2017) 1589–1591, https://doi.org/10.1007/s10439-017-1862-0.

[12] C.D. Cook, A.S. Hill, M. Guo, L. Stockdale, J.P. Papps, K.B. Isaacson, D.A. Lauffenburger, L.G. Griffith, Local remodeling of synthetic extracellular matrix microenvironments by co-cultured endometrial epithelial and stromal cells enables long-term dynamic physiological function, Integr. Biol. Quant. Biosci. Nano Macro. 9 (2017) 271–289, https://doi.org/10.1039/c6ib00245e.

[13] H. Yang, S. Wu, R. Feng, J. Huang, L. Liu, F. Liu, Y. Chen, Vitamin C plus hydrogel facilitates bone marrow stromal cell-mediated endometrium regeneration in rats, Stem Cell Res. Ther. 8 (2017) 267, https://doi.org/10.1186/s13287-017-0718-8.

[14] L. Ding, X. Li, H. Sun, J. Su, N. Lin, B. Péault, T. Song, J. Yang, J. Dai, Y. Hu, Transplantation of bone marrow mesenchymal stem cells on collagen scaffolds for the functional regeneration of injured rat uterus, Biomaterials 35 (2014) 4888–4900, https://doi.org/10.1016/j.biomaterials.2014.02.046.

[15] S.C. Schutte, C.O. James, N. Sidell, R.N. Taylor, Tissue-engineered endometrial model for the study of cell-cell interactions, Reprod. Sci. 22 (2015) 308–315, https://doi.org/10.1177/1933719114542008.

[16] R.C. Young, G. Goloman, Allo- and Xeno-reassembly of human and rat myometrium from cells and scaffolds, Tissue Eng. Part A 19 (2013) 2112–2119, https://doi.org/10.1089/ten.tea.2012.0549.

[17] M. Hellström, R.R. El-Akouri, C. Sihlbom, B.M. Olsson, J. Lengqvist, H. Bäckdahl, B.R. Johansson, M. Olausson, S. Sumitran-Holgersson, M. Brännström, Towards the development of a bioengineered uterus: comparison of different protocols for rat uterus decellularization, Acta Biomater. 10 (2014) 5034–5042, https://doi.org/10.1016/j.actbio.2014.08.018.

[18] K. Miyazaki, T. Maruyama, Partial regeneration and reconstruction of the rat uterus through recellularization of a decellularized uterine matrix, Biomaterials 35 (2014) 8791–8800, https://doi.org/10.1016/j.biomaterials.2014.06.052.

[19] P.M. Crapo, T.W. Gilbert, S.F. Badylak, An overview of tissue and whole organ decellularization processes, Biomaterials 32 (2011) 3233–3243, https://doi.org/10.1016/j.biomaterials.2011.01.057.

[20] J.D. O'Neill, R. Anfang, A. Anandappa, J. Costa, J.J. Javidfar, H.M. Wobma, G. Singh, D.O. Freytes, M.D. Bacchetta, J.R. Sonett, G. Vunjak-Novakovic, Decellularization of human and porcine lung tissues for pulmonary tissue engineering, Ann. Thorac. Surg. 96 (2013) 1046–1056, https://doi.org/10.1016/j.athoracsur.2013.04.022.
[21] D.C. Sullivan, S.-H. Mirmalek-Sani, D.B. Deegan, P.M. Baptista, T. Aboushwareb, A. Atala, J.J. Yoo, Decellularization methods of porcine kidneys for whole organ engineering using a high-throughput system, Biomaterials 33 (2012) 7756–7764, https://doi.org/10.1016/j.biomaterials.2012.07.023.
[22] P.M. Baptista, D. Vyas, E. Moran, Z. Wang, S. Soker, Human liver bioengineering using a whole liver decellularized bioscaffold, Methods Mol. Biol. Clifton NJ. 1001 (2013) 289–298, https://doi.org/10.1007/978-1-62703-363-3_24.
[23] H.C. Ott, T.S. Matthiesen, S.-K. Goh, L.D. Black, S.M. Kren, T.I. Netoff, D.A. Taylor, Perfusion-decellularized matrix: using nature's platform to engineer a bioartificial heart, Nat. Med. 14 (2008) 213–221, https://doi.org/10.1038/nm1684.
[24] H. Campo, P.M. Baptista, N. López-Pérez, A. Faus, I. Cervelló, C. Simón, De and recellularization of the pig uterus: a bioengineering pilot study, Biol. Reprod. (2016).
[25] M. Hellström, J.M. Moreno-Moya, S. Bandstein, E. Bom, R.R. Akouri, K. Miyazaki, T. Maruyama, M. Brännström, Bioengineered uterine tissue supports pregnancy in a rat model, Fertil. Steril. 106 (2016) 487–496.e1, https://doi.org/10.1016/j.fertnstert.2016.03.048.
[26] E.G. Santoso, K. Yoshida, Y. Hirota, M. Aizawa, O. Yoshino, A. Kishida, Y. Osuga, S. Saito, T. Ushida, K.S. Furukawa, Application of detergents or high hydrostatic pressure as decellularization processes in uterine tissues and their subsequent effects on in vivo uterine regeneration in murine models, PLoS One 9 (2014), https://doi.org/10.1371/journal.pone.0103201 e103201.
[27] G. Agmon, K.L. Christman, Controlling stem cell behavior with decellularized extracellular matrix scaffolds, Curr. Opin. Solid State Mater. Sci. 20 (2016) 193–201, https://doi.org/10.1016/j.cossms.2016.02.001.
[28] I. Cervelló, A. Mas, C. Gil-Sanchis, L. Peris, A. Faus, P.T.K. Saunders, H.O.D. Critchley, C. Simón, Reconstruction of endometrium from human endometrial side population cell lines, PLoS One 6 (2011), https://doi.org/10.1371/journal.pone.0021221.
[29] D. Vyas, P.M. Baptista, M. Brovold, E. Moran, B. Gaston, C. Booth, M. Samuel, A. Atala, S. Soker, Self-assembled liver organoids recapitulate hepatobiliary organogenesis in vitro, Hepatology 67 (2018) 750–761, https://doi.org/10.1002/hep.29483.
[30] D.A. Foyt, M.D.A. Norman, T.T.L. Yu, E. Gentleman, Exploiting advanced hydrogel technologies to address key challenges in regenerative medicine, Adv. Healthc. Mater. 7 (2018), https://doi.org/10.1002/adhm.201700939 e1700939.
[31] K.M. French, A.V. Boopathy, J.A. DeQuach, L. Chingozha, H. Lu, K.L. Christman, M.E. Davis, A naturally derived cardiac extracellular matrix enhances cardiac progenitor cell behavior in vitro, Acta Biomater. 8 (2012) 4357–4364, https://doi.org/10.1016/j.actbio.2012.07.033.
[32] X. Zhang, J. Dong, Direct comparison of different coating matrix on the hepatic differentiation from adipose-derived stem cells, Biochem. Biophys. Res. Commun. 456 (2015) 938–944, https://doi.org/10.1016/j.bbrc.2014.11.004.
[33] D.A. Young, Y.S. Choi, A.J. Engler, K.L. Christman, Stimulation of adipogenesis of adult adipose-derived stem cells using substrates that mimic the stiffness of adipose tissue, Biomaterials 34 (2013) 8581–8588, https://doi.org/10.1016/j.biomaterials.2013.07.103.
[34] J.A. DeQuach, S.H. Yuan, L.S.B. Goldstein, K.L. Christman, Decellularized porcine brain matrix for cell culture and tissue engineering scaffolds, Tissue Eng. Part A 17 (2011) 2583–2592, https://doi.org/10.1089/ten.tea.2010.0724.
[35] B. Fischer, P. Chavatte-Palmer, C. Viebahn, A. Navarrete Santos, V. Duranthon, Rabbit as a reproductive model for human health, Reprod. Camb. Engl. 144 (2012) 1–10, https://doi.org/10.1530/REP-12-0091.
[36] D.O. Freytes, J. Martin, S.S. Velankar, A.S. Lee, S.F. Badylak, Preparation and rheological characterization of a gel form of the porcine urinary bladder matrix, Biomaterials 29 (2008) 1630–1637, https://doi.org/10.1016/j.biomaterials.2007.12.014.
[37] A. Shevchenko, O.N. Jensen, A.V. Podtelejnikov, F. Sagliocco, M. Wilm, O. Vorm, P. Mortensen, A. Shevchenko, H. Boucherie, M. Mann, Linking genome and proteome by mass spectrometry: large-scale identification of yeast proteins from two dimensional gels, Proc. Natl. Acad. Sci. USA 93 (1996) 14440–14445.
[38] I.V. Shilov, S.L. Seymour, A.A. Patel, A. Loboda, W.H. Tang, S.P. Keating, C.L. Hunter, L.M. Nuwaysir, D.A. Schaeffer, The Paragon Algorithm, a next generation search engine that uses sequence temperature values and feature probabilities to identify peptides from tandem mass spectra, Mol. Cell. Proteomics MCP 6 (2007) 1638–1655, https://doi.org/10.1074/mcp.T600050-MCP200.
[39] M.T. Wolf, K.A. Daly, E.P. Brennan-Pierce, S.A. Johnson, C. Carruthers, A. D'Amore, S.P. Nagarkar, S.S. Velankar, S.F. Badylak, A hydrogel derived from decellularized dermal extracellular matrix, Biomaterials 33 (2012) 7028–7038, https://doi.org/10.1016/j.biomaterials.2012.06.051.
[40] M.P. Viudes-de-Castro, F. Marco-Jiménez, J.I. Cedano-Castro, J.S. Vicente, Effect of corifollitropin alfa supplemented with or without LH on ovarian stimulation and embryo viability in rabbit, Theriogenology 98 (2017) 68–74, https://doi.org/10.1016/j.theriogenology.2017.05.005.
[41] L. Llobat, F. Marco-Jiménez, D.S. Peñaranda, M.D. Saenz-de-Juano, J.S. Vicente, effect of embryonic genotype on reference gene selection for RT-qPCR normalization, Reprod. Domest. Anim. Zuchthyg. 47 (2012) 629–634, https://doi.org/10.1111/j.1439-0531.2011.01934.x.
[42] A. Blasco, The use of Bayesian statistics in meat quality analyses: a review, Meat Sci. 69 (2005) 115–122, https://doi.org/10.1016/j.meatsci.2004.06.012.
[43] K. Hodge, S.T. Have, L. Hutton, A.I. Lamond, Cleaning up the masses: exclusion lists to reduce contamination with HPLC-MS/MS, J. Proteomics 88 (2013) 92–103, https://doi.org/10.1016/j.jprot.2013.02.023.
[44] S.L. Voytik-Harbin, A.O. Brightman, B.Z. Waisner, J.P. Robinson, C.H. Lamar, Small intestinal submucosa: a tissue-derived extracellular matrix that promotes tissue-specific growth and differentiation of cells in vitro, Tissue Eng. 4 (1998) 157–174, https://doi.org/10.1089/ten.1998.4.157.
[45] L.T. Saldin, M.C. Cramer, S.S. Velankar, L.J. White, S.F. Badylak, Extracellular matrix hydrogels from decellularized tissues: structure and function, Acta Biomater. 49 (2017) 1–15, https://doi.org/10.1016/j.actbio.2016.11.068.
[46] C. Chiti, V. Aiswarya, J. Vanacker, L. Germain, L.J. White, M.-M. Dolmans, A. Des Rieux, C.A. Amorim, Hydrogel from bovine decellularized ovarian extracellular matrix supports mouse follicle survival in vitro Front, Bioeng. Biotechnol. (2016), https://doi.org/10.3389/conf.FBIOE.2016.01.00014.
[47] L.H. Friedrich, P. Jungebluth, S. Sjöqvist, V. Lundin, J.C. Haag, G. Lemon, Y. Gustafsson, F. Ajallouеian, A. Sotnichenko, H. Kielstein, M.A. Burguillos, B. Joseph, A.I. Teixeira, M.L. Lim, P. Macchiarini, Preservation of aortic root architecture and properties using a detergent-enzymatic perfusion protocol, Biomaterials 35 (2014) 1907–1913, https://doi.org/10.1016/j.biomaterials.2013.11.053.
[48] M. Lorvellec, F. Scottoni, C. Crowley, R. Fiadeiro, P. Maghsoudlou, A.F. Pellegata, F. Mazzacuva, A. Gjinovci, A.-M. Lyne, J. Zulini, D. Little, O. Mosaku, D. Kelly, P. D. Coppi, P. Gissen, Mouse decellularised liver scaffold improves human embryonic and induced pluripotent stem cells differentiation into hepatocyte-like cells, PLoS One 12 (2017), https://doi.org/10.1371/journal.pone.0189586 e0189586.
[49] Y. Miyauchi, K. Yasuchika, K. Fukumitsu, T. Ishii, S. Ogiso, T. Minami, H. Kojima, R. Yamaoka, H. Katayama, T. Kawai, E.Y. Yoshitoshi-Uebayashi, S. Kita, K. Yasuda, N. Sasaki, S. Uemoto, A novel three-dimensional culture system maintaining the physiological extracellular matrix of fibrotic model livers accelerates progression of hepatocellular carcinoma cells, Sci. Rep. 7 (2017) 9827, https://doi.org/10.1038/s41598-017-09391-y.
[50] G. Mazza, J.P. Simons, R. Al-Shawi, S. Ellmerich, L. Urbani, S. Giorgetti, G.W. Taylor, J.A. Gilbertson, A.R. Hall, W. Al-Akkad, D. Dhar, P.N. Hawkins, P. De Coppi, M. Pinzani, V. Bellotti, P.P. Mangione, Amyloid persistence in decellularized liver: biochemical and histopathological characterization, Amyloid 23 (2016) 1–7, https://doi.org/10.3109/13506129.2015.1110518.
[51] P.P. Mangione, G. Mazza, J.A. Gilbertson, N.B. Rendell, D. Canetti, S. Giorgetti, L. Frenguelli, M. Curti, T. Rezk, S. Raimondi, M.B. Pepys, P.N. Hawkins, J.D. Gillmore, G.W. Taylor, M. Pinzani, V. Bellotti, Increasing the accuracy of proteomic typing by decellularisation of amyloid tissue biopsies, J. Proteomics 165 (2017) 113–118, https://doi.org/10.1016/j.jprot.2017.06.016.
[52] M.L. Pinto, E. Rios, A.C. Silva, S.C. Neves, H.R. Caires, A.T. Pinto, C. Durães, F.A. Carvalho, A.P. Cardoso, N.C. Santos, C.C. Barrias, D.S. Nascimento, P. Pinto-do-Ó, M.A. Barbosa, F. Carneiro, M.J. Oliveira, Decellularized human colorectal cancer matrices polarize macrophages towards an anti-inflammatory phenotype promoting cancer cell invasion via CCL18, Biomaterials 124 (2017) 211–224, https://doi.org/10.1016/j.biomaterials.2017.02.004.
[53] M. Piccoli, E. D'Angelo, S. Crotti, F. Sensi, L. Urbani, E. Maghin, A. Burns, P.D. Coppi, M. Fassan, M. Rugge, F. Rizzolio, A. Giordano, P. Pilati, E. Mammano, S. Pucciarelli, M. Agostini, Decellularized colorectal cancer matrix as bioactive microenvironment for in vitro 3D cancer research, J. Cell. Physiol. 233 (2018) 5937–5948, https://doi.org/10.1002/jcp.26403.
[54] D. Sood, K. Chwalek, E. Stuntz, D. Pouli, C. Du, M. Tang-Schomer, I. Georgakoudi, L.D. Black, D.L. Kaplan, Fetal brain extracellular matrix boosts neuronal network formation in 3D bioengineered model of cortical brain tissue, ACS Biomater. Sci. Eng. 2 (2016) 131–140, https://doi.org/10.1021/acsbiomaterials.5b00446.
[55] H.N. Jabbour, R.W. Kelly, H.M. Fraser, H.O.D. Critchley, Endocrine regulation of menstruation, Endocr. Rev. 27 (2006) 17–46, https://doi.org/10.1210/er.2004-0021.
[56] J. Evans, T. Kaitu'u-Lino, L.A. Salamonsen, Extracellular matrix dynamics in scar-free endometrial repair: perspectives from mouse in vivo and human in vitro studies, Biol. Reprod. 85 (2011) 511–523, https://doi.org/10.1095/biolreprod.111.090993.
[57] G. Jones, A. Herbert, H. Berry, J.H. Edwards, J. Fisher, E. Ingham, Decellularization and characterization of porcine superflexor tendon: a potential anterior cruciate ligament replacement, Tissue Eng. Part A 23 (2017) 124–134, https://doi.org/10.1089/ten.tea.2016.0114.
[58] D.J. Harrington, B.A. Lessey, V. Rai, A. Bergqvist, S. Kennedy, S. Manek, D.H. Barlow, H.J. Mardon, Tenascin is differentially expressed in endometrium and endometriosis, J. Pathol. 187 (1999) 242–248, https://doi.org/10.1002/(SICI)1096-9896(199901)187:2<242::AID-PATH221>3.0.CO;2-T.
[59] M. Yamanaka, M. Taga, H. Minaguchi, Immunohistological localization of tenascin in the human endometrium, Gynecol. Obstet. Invest. 41 (1996) 247–252, https://doi.org/10.1159/000292279.
[60] K.S. Midwood, M. Chiquet, R.P. Tucker, G. Orend, Tenascin-C at a glance, J Cell Sci. 129 (2016) 4321–4327, https://doi.org/10.1242/jcs.190546.
[61] Z.S. Patel, A.G. Mikos, Angiogenesis with biomaterial-based drug- and cell-delivery systems, J. Biomater. Sci. Polym. Ed. 15 (2004) 701–726.
[62] J. Ishihara, A. Ishihara, K. Fukunaga, K. Sasaki, M.J.V. White, P.S. Briquez, J.A. Hubbell, Laminin heparin-binding peptides bind to several growth factors and enhance diabetic wound healing, Nat. Commun. 9 (2018) 2163, https://doi.org/10.1038/s41467-018-04525-w.

[63] M. Oakes, L. Cabrera, H. Nanadivada, J. Lahann, G. Smith, Effects of 3-Dimensional Topography, Dynamic Fluid Movement and an Insoluble Glycoprotein Matrix on Murine Embyro Development, Proc. SGI Annu. Meet., Glasgow, Scotland, 2009.
[64] I.N. Simões, P. Vale, S. Soker, A. Atala, D. Keller, R. Noiva, S. Carvalho, C. Peleteiro, J.M.S. Cabral, D. Eberli, C.L. da Silva, P.M. Baptista, Acellular urethra bioscaffold: decellularization of whole urethras for tissue engineering applications, Sci. Rep. 7 (2017), https://doi.org/10.1038/srep41934.
[65] C. González-García, M. Cantini, J. Ballester-Beltrán, G. Altankov, M. Salmerón-Sánchez, The strength of the protein-material interaction determines cell fate, Acta Biomater. 77 (2018) 74–84, https://doi.org/10.1016/j.actbio.2018.07.016.
[66] H.-W. Denker, Proteases of the Blastocyst and of the Uterus, in: H.M. Beier, P. Karlson (Eds.), Proteins Steroids Early Pregnancy, Springer, Berlin Heidelberg, 1982, pp. 183–208.
[67] V. Chickarmane, C. Troein, U.A. Nuber, H.M. Sauro, C. Peterson, Transcriptional dynamics of the embryonic stem cell switch, PLoS Comput. Biol. 2 (2006), https://doi.org/10.1371/journal.pcbi.0020123 e123.
[68] S. Okumura-Nakanishi, M. Saito, H. Niwa, F. Ishikawa, Oct-3/4 and Sox2 regulate Oct-3/4 gene in embryonic stem cells, J. Biol. Chem. 280 (2005) 5307–5317, https://doi.org/10.1074/jbc.M410015200.
[69] M. Keramari, J. Razavi, K.A. Ingman, C. Patsch, F. Edenhofer, C.M. Ward, S.J. Kimber, Sox2 is essential for formation of trophectoderm in the preimplantation Embryo, PLoS One 5 (2010), https://doi.org/10.1371/journal.pone.0013952.
[70] L.S. Kumosa, V. Zetterberg, J. Schouenborg, Gelatin promotes rapid restoration of the blood brain barrier after acute brain injury, Acta Biomater. 65 (2018) 137–149, https://doi.org/10.1016/j.actbio.2017.10.020.
[71] D.M. Faulk, R. Londono, M.T. Wolf, C.A. Ranallo, C.A. Carruthers, J.D. Wildemann, C.L. Dearth, S.F. Badylak, ECM hydrogel coating mitigates the chronic inflammatory response to polypropylene mesh, Biomaterials 35 (2014) 8585–8595, https://doi.org/10.1016/j.biomaterials.2014.06.057.
[72] S.B. Seif-Naraghi, J.M. Singelyn, M.A. Salvatore, K.G. Osborn, J.J. Wang, U. Sampat, O.L. Kwan, G.M. Strachan, J. Wong, P.J. Schup-Magoffin, R.L. Braden, K. Bartels, J.A. DeQuach, M. Preul, A.M. Kinsey, A.N. DeMaria, N. Dib, K.L. Christman, Safety and efficacy of an injectable extracellular matrix hydrogel for treating myocardial infarction, Sci. Transl. Med. 5 (2013), https://doi.org/10.1126/scitranslmed.3005503.
[73] D. Gothard, E.L. Smith, J.M. Kanczler, C.R. Black, J.A. Wells, C.A. Roberts, L.J. White, O. Qutachi, H. Peto, H. Rashidi, L. Rojo, M.M. Stevens, A.J.E. Haj, F.R.A.J. Rose, K.M. Shakesheff, R.O.C. Oreffo, In vivo assessment of bone regeneration in Alginate/Bone ECM hydrogels with incorporated skeletal stem cells and single growth factors, PLoS One 10 (2015), https://doi.org/10.1371/journal.pone.0145080 e0145080.
[74] S.B. Seif-Naraghi, D. Horn, P.J. Schup-Magoffin, K.L. Christman, Injectable extracellular matrix derived hydrogel provides a platform for enhanced retention and delivery of a heparin-binding growth factor, Acta Biomater. 8 (2012) 3695–3703, https://doi.org/10.1016/j.actbio.2012.06.030.
[75] X. Santamaria, S. Cabanillas, I. Cervelló, C. Arbona, F. Raga, J. Ferro, J. Palmero, J. Remohí, A. Pellicer, C. Simón, Autologous cell therapy with CD133+ bone marrow-derived stem cells for refractory Asherman's syndrome and endometrial atrophy: a pilot cohort study, Hum. Reprod. Oxf. Engl. 31 (2016) 1087–1096, https://doi.org/10.1093/humrep/dew042.
[76] S.F. Badylak, D.O. Freytes, T.W. Gilbert, Extracellular matrix as a biological scaffold material: structure and function, Acta Biomater. 5 (2009) 1–13, https://doi.org/10.1016/j.actbio.2008.09.013.